Astronomy & Astrophysics manuscript no. axper˙mar11
March 25, 2011

Formation of a disk structure in the symbiotic binary AX Per during its 2007-10 precursor-type activity

A. Skopal⋆[1], T. Tarasova[2], Z. Cariková[1], F. Castellani[3], G. Cherini[3], S. Dallaporta[3], A. Frigo[3], C. Marangoni[3], S. Moretti[4], U. Munari[4], G. L. Righetti[3], A. Siviero[5], S. Tomaselli[3], A. Vagnozzi[3], and P. Valisa[3]

[1] Astronomical Institute, Slovak Academy of Sciences, 059 60 Tatranská Lomnica, Slovakia
[2] Crimean Astrophysical Observatory, Nauchny, Ukraine
[3] ANS Collaboration, c/o Osservatorio Astronomico di Padova, Sede di Asiago, I-36032 Asiago (VI), Italy
[4] INAF Osservatorio Astronomico di Padova, Sede di Asiago, I-36032 Asiago (VI), Italy
[5] Dipartimento di Astronomia, Universita' di Padova, Osservatorio Astrofisico, I-36012 Asiago (VI), Italy

Received / Accepted

ABSTRACT

Context. AX Per is an eclipsing symbiotic binary. During active phases, deep narrow minima are observed in its light curve, and the ionization structure in the binary changes significantly. From ~2007.5, AX Per entered a new active phase.
Aims. We identified formation of a neutral disk structure around the hot star as a result of its enhanced wind during the active phase.
Methods. We used optical high- and low-resolution spectroscopy and $UBVR_CI_C$ photometry. We modeled the SED in the optical, broad wings of the Hα line, and analyzed the multicolour photometry during the 2007-10 higher level of the AX Per activity.
Results. After 10 orbital cycles (~ 18.6 years), we measured again in the light curve the eclipse of the hot active object by its giant companion. We derived a radius of $27 \pm 2\,R_\odot$ for the eclipsed object and $115 \pm 2\,R_\odot$ for the eclipsing cool giant, the latter being within 10% of what measured during the 1988-1990 outburst. New active phase was connected with a significant enhancement of the hot star wind. From quiescence to activity, the mass loss rate increased from $\sim 9 \times 10^{-8}$ to $\sim 3 \times 10^{-6}\,M_\odot\,\mathrm{yr}^{-1}$, respectively. The wind gives rise to the emission of the He^{++} zone, located at the vicinity of the hot star, and to a fraction of the [O III] zone at farther distances. Simultaneously, we identified a neutral, $T_{\rm eff} \sim 6000$ K warm, stellar source contributing markedly to the composite spectrum. The source was located at the hot star's equator and had a form of a flared disk, which outer rim simulated the warm photosphere.
Conclusions. Formation of the neutral disk-like zone around the accretor during the active phase was connected with its enhanced wind. Probably, this connection represents a common origin of cool pseudophotospheres indicated during active phases of symbiotic stars.

Key words. Accretion, accretion discs – stars: binaries: symbiotic – stars: winds, outflows – stars: individual: AX Per

1. Introduction

Symbiotic stars are interacting binary systems comprising a cool giant and a compact star, mostly a white dwarf (WD), on, typically, a few years orbit. The WD accretes from the giant's wind, heats up to 1–2×10^5 K, and becomes as luminous as 10^2 – $10^4\,L_\odot$. It ionizes the circumbinary environment giving rise to nebular emission. As a result the spectrum of symbiotic stars consists of three basic components of radiation – two stellar and one nebular. If the processes of the mass-loss, accretion and ionization are in a mutual equilibrium, then symbiotic system releases its energy approximately at a constant rate and spectral energy distribution (SED). This stage is called as the *quiescent phase*. Once this equilibrium is disturbed, symbiotic system changes its radiation significantly, brightens up in the optical by a few magnitudes and usually shows signatures of a mass-outflow for a few months to years. We name this stage as the *active phase*. Many particular aspects of this general view have been originally pointed by, e.g., Seaquist et al. (1984) and Nussbaumer & Vogel (1989), and more recently discussed in Corradi et al. (2003).

The key problem in the symbiotic star research is the understanding the nature of their outbursts. At present, theories of thermonuclear runaways and instabilities of accretion disk do not allow to explain the short recurrence time (from years to decades) and low luminosity of the outbursts produced by symbiotic systems. Recently, Sokoloski et al. (2006) attempted to solve this problem by combining effects of both a disk instability and a thermonuclear burning, while Bisikalo et al. (2006) suggested a disruption of the disk due to variations in the velocity of the wind from the giant, and proposed formation of a system of shocks to explain the star's brightness. Originally, Tutukov & Yangelson (1976), Paczyński & Żytkow (1978), Fujimoto (1982) and Paczyński & Rudak (1980) proposed that most symbiotic stars are powered by stable hydrogen nuclear burning on the WD surface. As the stable burning requires a rather narrow range of the accretion rate, the burning envelope will react with an expansion to any increase in the accretion rate above that sustaining the stable burning (see summary by Mikolajewska & Kenyon 1992a). As a result, the pseudophotosphere will radiate at lower temperature, and thus shift the maximum of its SED from shorter to longer wavelengths, causing a brightening in the optical. This scenario was supported by, for example, Munari & Buson (1994) and Siviero et al. (2009). A study of rapid variability in symbiotic stars indicated the presence of disks during outbursts (e.g. Sokoloski 2003). In addition, observational evidence for a disk-jet connection in CH Cyg (Sokoloski & Kenyon 2003) and Z And (Skopal et al. 2009a) strongly supported the

⋆ Visiting Astronomer: Asiago Astrophysical Observatory

presence of a massive disk during active phases of these objects. Independently, modeling the UV/IR SED for 21 symbiotic stars also indicated the presence of a flared disk around the accretor during active phases (Skopal 2005).

In this contribution we investigate the recent, 2007-10, higher level of the AX Per activity with the main goal to understand better formation of the disk-like structure around its accretor. At present, AX Per is known as an eclipsing symbiotic binary comprising a M4.5 III giant (Mürset & Schmid 1999) and a WD on a 680-d orbit (e.g. Skopal 1991; Mikolajewska & Kenyon 1992b; Fekel et al. 2000). The last active phase began in 1988, when AX Per brightened by ∼3 mag in the visual, developed a specific phase-dependent modulation in the LC, and showed narrow eclipses at the position of the inferior conjunction of the giant (Skopal et al. 2001, Fig. 1 here). Transition to quiescence happened during 1995, when the LC profile turned to the wave-like orbitally-related variation at a low level of the star's brightness.

Our photometric monitoring programmes, performed by ANS (Asiago Novae and Symbiotic Stars) Collaboration and at Skalnaté Pleso Observatory, revealed an anomalous variation in the LC of AX Per from around 2007. In particular, Munari et al. (2009) reported on a rapid increase in brightness by ∼1 mag in *B* during 2009 March. They pointed a similarity between this brightening phase and the short-duration flare that occurred in the AX Per LC about one year before its major, 1988-1995, active phase. Recently, Munari et al. (2010) reported on a rise in brightness of AX Per during 2010 November by ∼0.7 mag in *B*, which thus supported their previous suggestion that the 2007-2010 active phase was a precursor to an oncoming major outburst. From this point of view, understanding the precursor-type activity can aid us to reveal the nature of the Z And-type outbursts.

Accordingly, in this paper we investigate the origin of the 2007-2010 brighter phase of AX Per by analyzing our multicolour photometric observations and the low- and high-resolution optical spectra. In Sect. 2 we summarize and describe our observations and data reduction. Section 3 describes our analysis and presents the results. Their discussion and conclusions are found in Sects. 4 and 5, respectively.

2. Observations and data reduction

Our observations of AX Per during its 2007-2010 higher level of activity were carried out at different observatories.

Spectroscopic observations were secured with five different instruments: (1) the 1.22-m telescope, operated in Asiago by the Department of Astronomy of the University of Padova, was used with a B&C spectrograph, 300 ln/mm grating and ANDOR iDus 440A CCD camera, equipped with a EEV 42-10BU back illuminated chip (2048×512 pixels of 13.5 μm size); (2) the 1.82-m telescope, operated in Asiago by INAF Astronomical Observatory of Padova, mounting a REOSC echelle spectrograph equipped with a AIMO E2VCCD47-10 back illuminated CCD detector (1100×1100 pixels of 13 μm size); (3) the 0.60-m telescope, of the Schiaparelli Observatory in Varese, mounting a multi-mode spectrograph, able to provide both single dispersion, low-resolution spectra as well as Echelle spectra. The detector was a SBIG ST-10XME camera (2194×51472 pixels of 6.8 μm size); (4) the 1.88-m telescope of the David Dunlap Observatory (DDO), University of Toronto (DDO), equipped with a single dispersion spectrograph equipped with a Jobin Yovon Horiba CCD detector (2048×512 pixels of 13.5 μm size); and finally (5) the 2.6-m Shajn telescope, operated by the Crimean Astrophysical Observatory (CrAO) in Nauchny, mounting a SPEM spectrograph in the Nasmith focus. The detector was a SPEC-10 CCD camera (1340×100 pixel). Table 1 provides a journal of the spectroscopic observations. At each telescope the observations were carried out as multiple exposures to avoid saturation of the strongest emission lines. Various spectrophotometric standards were observed each night to flux into absolute units the spectra of AX Per. The accuracy of the flux scale was checked against the photometric observations by integration over the fluxed spectra of the $UBVR_{\rm C}I_{\rm C}$ photometric pass-bands. Correction for flat, bias and dark frames was carried out in a standard way with IRAF, as well subtraction of the background sky and scattered light.

Table 1. Log of spectroscopic observations

Date	Julian date +2450000	Res. Power	Disp. (Å/pix)	λ range (Å)	Telescope
2007/07/31	4312.876	10 000		Hβ, Hα	DDO 1.88m
2007/11/20	4425.529		1.81	3824- 7575	CrAO 2.6m
2007/12/03	4438.438		2.30	3230- 7770	Asiago 1.22m
2008/01/23	4488.506	10 000		Hβ, Hα	DDO 1.88m
2008/07/07	4655.473		1.81	3774- 7574	CrAO 2.6m
2008/08/10	4689.450		1.81	3749- 7575	CrAO 2.6m
2008/09/24	4734.609		1.81	3749- 7575	CrAO 2.6m
2008/10/13	4753.638	20 000		3690- 7300	Asiago 1.82m
2008/10/23	4763.417		1.81	3349- 7149	CrAO 2.6m
2008/11/08	4778.393		1.81	3749- 7500	CrAO 2.6m
2008/12/08	4809.390		2.30	3250- 7830	Asiago 1.22m
2008/12/21	4822.437	20 000		3690- 7300	Asiago 1.82m
2009/01/09	4841.426	20 000		3690- 7300	Asiago 1.82m
2009/03/24	4915.422		2.12	3890- 7930	Varese 0.60m
2009/04/01	4923.323		2.30	4200- 7200	Asiago 1.22m
2009/04/07	4929.303		2.12	3900- 8120	Varese 0.60m
2009/04/08	4930.301		2.30	3340- 7620	Asiago 1.22m
2009/04/09	4931.262		1.81	3600- 7575	CrAO 2.6m
2009/04/14	4936.281		2.30	3560- 7580	Asiago 1.22m
2009/04/14	4936.338	17 000		4030- 7510	Varese 0.60m
2009/05/05	4957.458		2.12	3850- 8270	Varese 0.60m
2009/08/05	5049.535		2.30	3320- 7660	Asiago 1.22m
2009/08/26	5070.565		1.81	3324- 7493	CrAO 2.6m
2009/09/24	5099.584		1.81	3350- 7500	CrAO 2.6m
2009/11/10	5146.485	20 000		3690- 7300	Asiago 1.82m
2010/08/07	5416.368		2.12	3910- 8540	Varese 0.60m
2010/08/16	5425.564		1.81	3358- 7500	CrAO 2.6m
2010/08/21	5430.348	17 000		3950- 8640	Varese 0.60m
2010/09/14	5454.560		1.81	3274- 7574	CrAO 2.6m

Multicolour $BVR_{\rm C}I_{\rm C}$ CCD photometry was obtained with various telescope operated by ANS Collaboration. Treatments for flat, bias and dark frames was carried out in a standard way. Photometric calibration and correction for color equations was carried out against the photometric sequence calibrated by Henden & Munari (2006) around AX Per. The resulting data are presented in Table 2. Their uncertainties are the overall budget errors (which includes the Poissonian component and the transformation to the standard Landolt system). They are of a few $\times 0.01 - 0.001$ mag.

In addition, classical photoelectric *UBV* measurements were performed by a single-channel photometer mounted in the Cassegrain focus of 0.6-m reflector at the Skalnaté Pleso observatory Internal uncertainties of these one-day-mean measurements are of a few ×0.01 mag (see Skopal et al. 2011, in detail). Figure 1 displays historical light curve (LC) of AX Per from ∼1890 to the present, together with *UBV* measurements

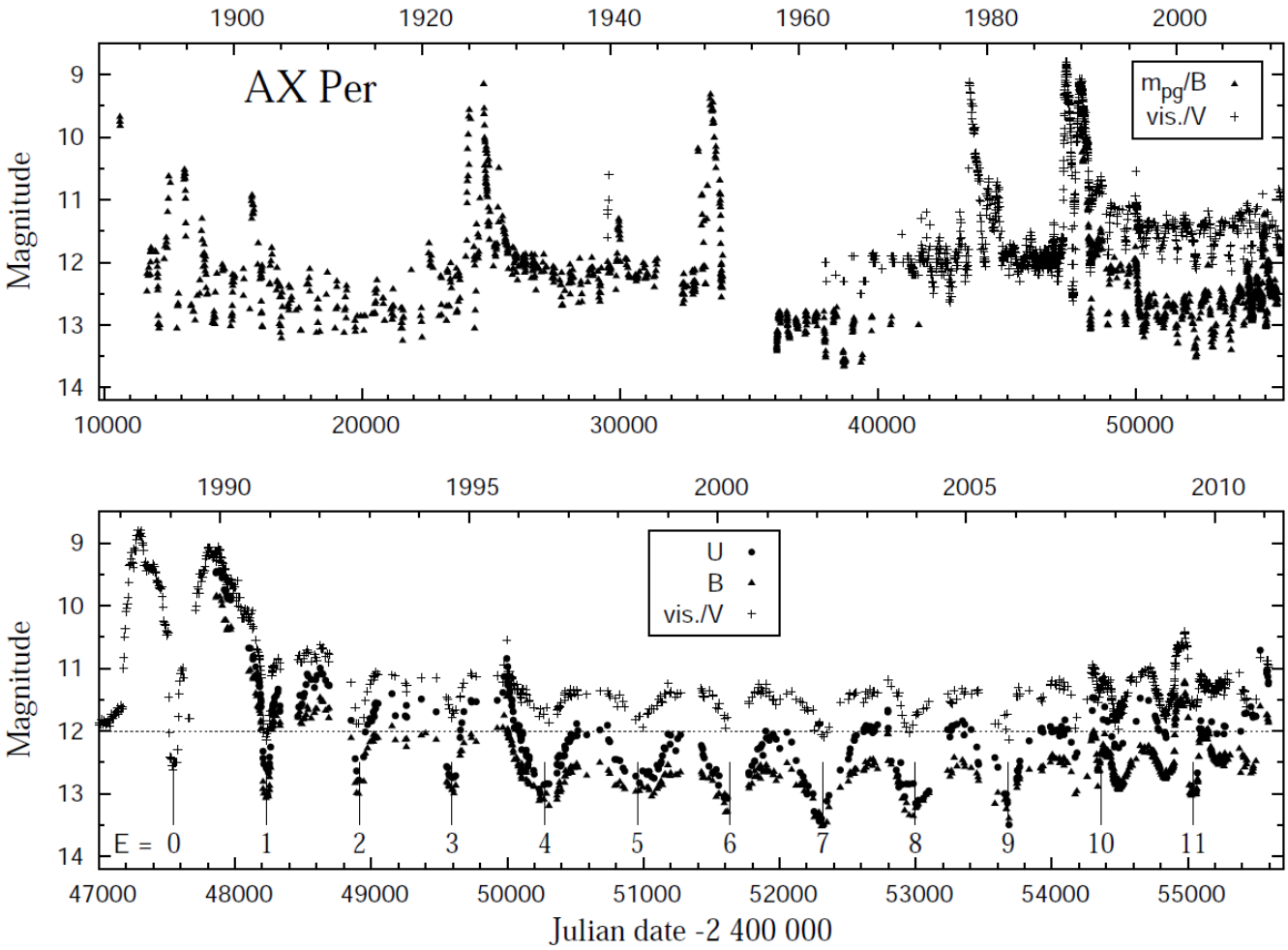

Fig. 1. Top panel displays the historical light curve (LC) of AX Per from ~1890 (see Fig. 1 of Skopal et al. 2001, and references therein). We used visual magnitude estimates from the AAVSO International Database and those gathered by members of the AFOEV, which are available on CDS. Visual data were smoothed within 20-day bins. Bottom panel shows the *UBV* LCs of AX Per from its last 1988 major outburst. Minima timing corresponds to the ephemeris given by Eq. (1).

recorded from its previous 1988-95 active phase. Figure 2 then shows its detail from 2007, covering the recent active phase.

Arbitrary flux units of the high-resolution spectra were converted to absolute fluxes with the aid of the simultaneous $UBVR_CI_C$ photometry corrected for emission lines (see Skopal 2007). To determine flux-points of the true continuum from the measured magnitudes, we calculated corrections, Δm_l, using our low-resolution spectra (Table 3). Then we interpolated these values to dates of high-resolution spectra. Relevant observations were dereddened with $E_{B-V} = 0.27$ (Kenyon & Webbink 1984) and resulting parameters were scaled to a distance of 1.73 kpc (Skopal 2000).

3. Analysis and results

3.1. Photometric evolution

3.1.1. Indications of a new active phase

According to the LC evolution from 1988 (Fig. 1), the increase in the star's brightness by ΔU ~0.5 mag from 2007 July, signals that AX Per entered a new active phase. An additional rapid brightening by ΔB ~0.8 mag and a bluer index $B - V \sim 0.8$, observed during 2009 March (Munari et al. 2009, and Fig. 2 here), supported the new activity of AX Per. Also a significant change of the broad minima, observed during quiescent phases at/around the giant inferior conjunction, into a narrower and deeper eclipses, indicates active phase of a symbiotic binary (e.g. Belyakina 1979, 1991, and Figs. 1 and 2 here). During the 2007 conjunction we measured a relatively small, V-type minimum, which position was shifted from the giant conjunction by $\sim -0.025\,P_{orb}$. During the following conjunction the eclipse was deeper and broader, nearly rectangular in profile and placed exactly at the inferior conjunction of the giant. The light observed during the totality became reder with $B - V \sim 1.4$ (see Fig. 2). Finally, we measured a puzzling wave in the LC with a period of $\sim 0.5\,P_{orb}$ and minima located around orbital phases 0.2 and 0.7. First indication of such the minimum preceded the 2007 eclipse. Its presence was transient, being connected only with the 2007-10 higher level of the star's activity (see Figs. 1 and 2). This feature was observed in a symbiotic system for the first time.

In the following sections (Sect. 3.1.2. to 3.1.4.) we analyze the most significant features in the LC profile and the nature of its light at different positions of the binary.

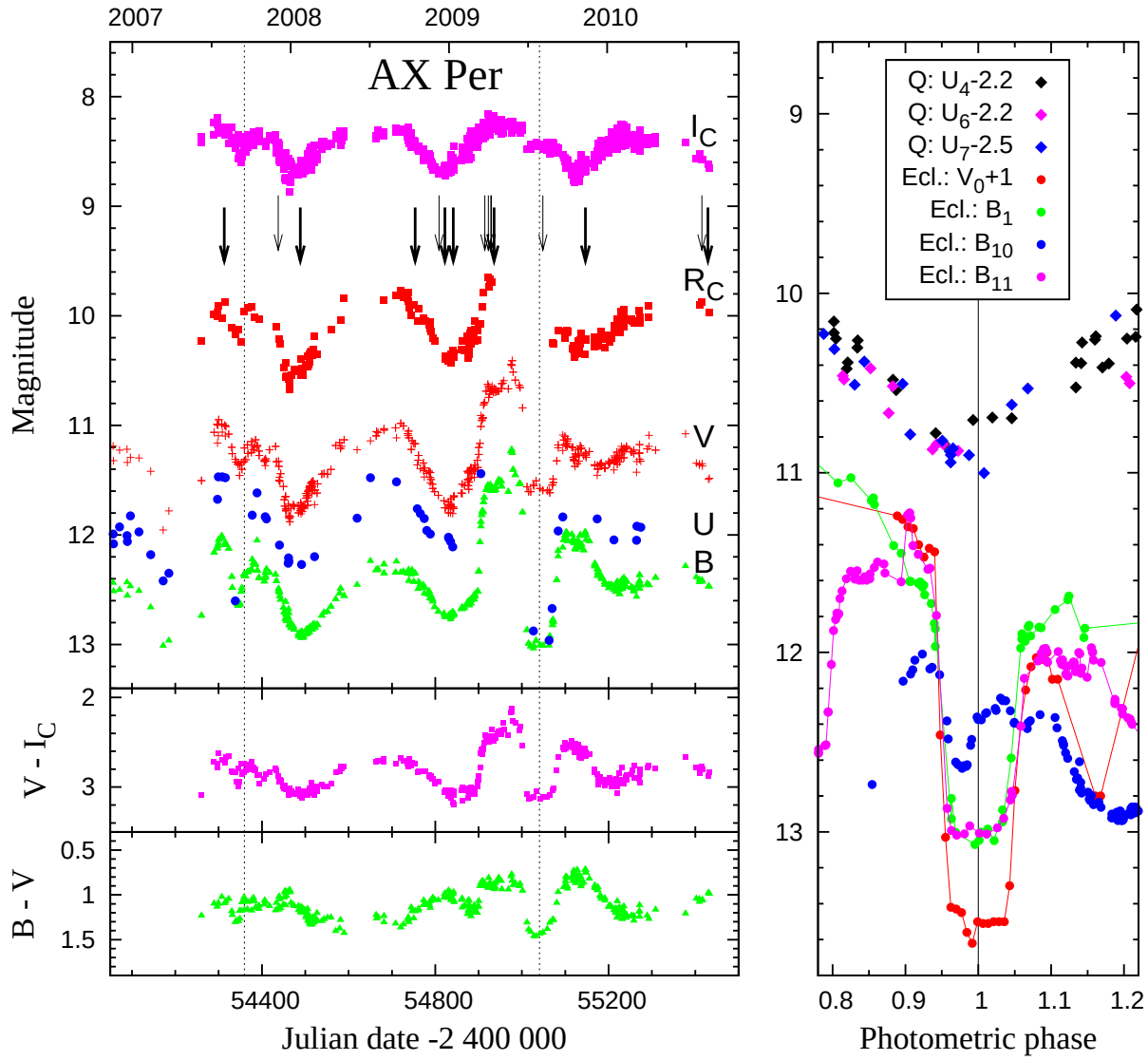

Fig. 2. Left: Recent $UBVR_CI_C$ LCs of AX Per covering its 2007-10 active phase. Thin and thick arrows denote the dates of our low- and high-resolution spectra, respectively (Table 1). Vertical dotted lines mark the time of eclipses according to Eq (1). Right: Minima profiles selected from LCs in Fig. 1, and folded with the ephemeris (1). Denotation in keys, for example "Q: U_4-2.2", means quiescent phase, U filter, epoch 4 and a shift by -2.2 mag.

3.1.2. Eclipses

The minimum (eclipse), observed during the 2009 brightening, was very similar in the profile to those observed during the major 1988-91 active phase. Its well pronounced profile closely covered by measurements, mainly in B and V bands, allowed us to determine its contact times as $T_1 = JD\ 2\,454\,998.50 \pm 0.79$, $T_2 = JD\ 2\,455\,012.50 \pm 0.53$, $T_3 = JD\ 2\,455\,065.40 \pm 0.85$ and $T_4 = JD\ 2\,455\,085.33 \pm 0.50$, where uncertainties include only those given by the data coverage, assuming a linear dependence of the star's brightness during the ingress to- and ascent from the totality. We neglected other possible sources of errors. These times and their uncertainties indicate an asymmetric profile with $T_2 - T_1 = 14 \pm 1.3$ d and $T_4 - T_3 = 20 \pm 1.3$ d, which implies an increase of the linear size of the eclipsed object during the totality. Therefore, we determined the middle of the eclipse as the average of all contact times, i.e. $JD_{\rm Ecl.}(2009) = JD\ 2\,455\,040.43 \pm 0.67$. Using well defined timings of other eclipses, $JD_{\rm Ecl.}(1989) = JD\ 2\,447\,551.7 \pm 1.0$ and $JD_{\rm Ecl.}(1990) = JD\ 2\,448\,231.6 \pm 0.6$ (Skopal 1991), gives their ephemeris as

$$JD_{\rm Ecl.} = 2\,447\,551.26(\pm 0.3) + 680.83(\pm 0.11) \times E. \qquad (1)$$

Our photometric ephemeris agrees within uncertainties with that given by the solution of the spectroscopic orbit, $T_{\rm sp.conj.} = 2\,447\,553.3(\pm 5.6) + 682.1(\pm 1.4) \times E$, obtained from infrared radial velocities by Fekel et al. (2000). Finally, assuming the orbital inclination $i = 90°$ and the separation between the binary components, $a = 364\,R_\odot$ (from the mass ratio and the mass function published by Mikolajewska & Kenyon 1992b; Fekel et al. 2000), the radius of the giant, $R_{\rm g} = 115 \pm 2\,R_\odot$ and that of the eclipsed object, $R_{\rm e} = 27 \pm 2\,R_\odot$. This result suggests an expansion of the giant radius by $\sim 13\,R_\odot$, from $102 \pm 3\,R_\odot$, given by contact times of the 1990 eclipse (Skopal 1994). However, due to possibly larger uncertainties in the contact times (see above), this suggestion should be taken with caution.

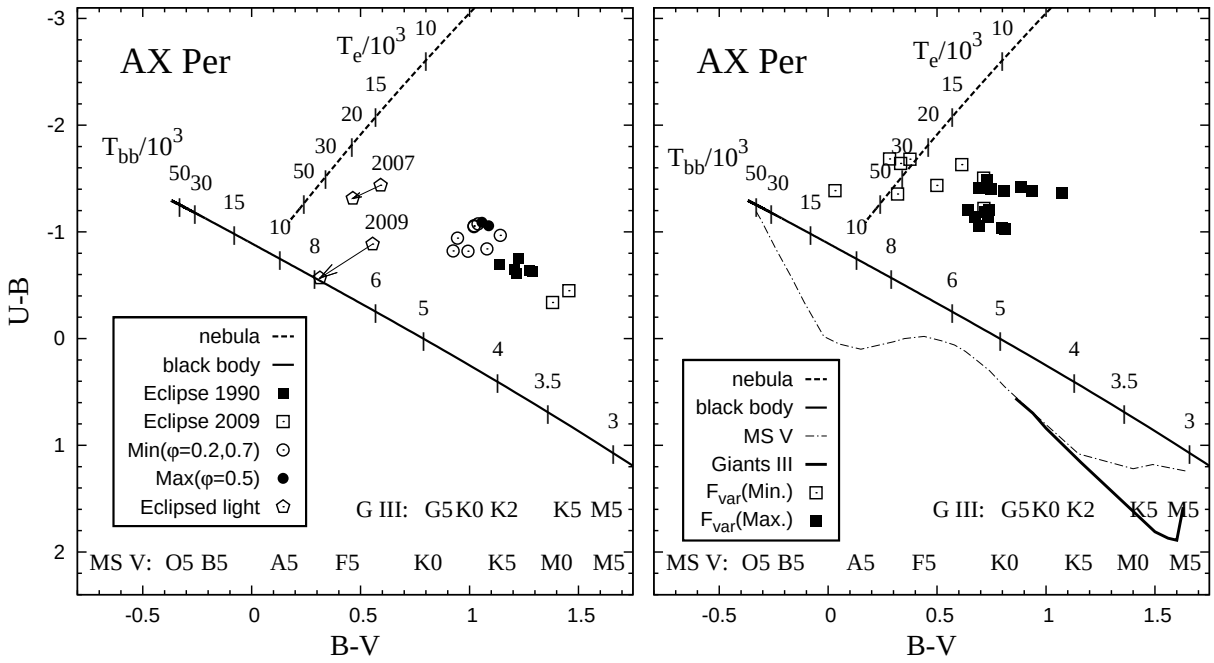

Fig. 3. Left: The $(U-B,\ B-V)$ diagram for the light observed (a) during the 2009 and 1990 eclipses (point (i) of Sect. 3.1.3), (b) at the minimum (2007/08 and 2008/09) and maximum (around 2008.6) of the LC (Fig. 2), and (c) eclipsed during the 2007 and 2009 inferior conjunction of the giant (point (ii) of Sect. 3.1.3). Right: The same as on the left, but for the variable light causing the puzzling wave in the LC (point (iii) of Sect. 3.1.3).

3.1.3. Colour indices

In this section we apply a $(U-B,\ B-V)$-diagram diagnostic to compare the observed colour indices to those of the continuum radiation produced by a stellar and nebular source of radiation. The former was approximated by a blackbody radiation and the latter by processes of recombination and thermal bremsstrahlung in the hydrogen plasma. We calculated theoretical colour indices in the same way as Skopal (2003). Here they are plotted in Fig. 3. The observed magnitudes were corrected for the interstellar extinction and the influence of emission lines to get the flux-points of the true continuum, and thus to be comparable with theoretical values. In particular, we applied the colour-index diagnostic to (i) the light observed during eclipses, (ii) the light, which is subject to eclipse, and (iii) the variable light causing the puzzling wave in the LC throughout the 2007-10 active phase. The following analysis could be carried out.

(i) In this case we used the *UBV* magnitudes from the 1990 and 2009 total eclipse. As expected, the $(U-B,\ B-V)$-diagram shows that the observed light during totality is composed of a contribution from the giant and a nebula (see Fig. 3, left panel). According to the positions of colour indices in the diagram, the light measured during the 1990 eclipse contained a stronger nebular contribution than that indicated for the 2009 eclipse, because of a relative shift to the line representing the net nebular radiation in the diagram. Corresponding physical parameters of the components of radiation seen in the spectrum during eclipses are estimated in Sect. 3.1.4.

(ii) The eclipsed flux, measured within the filter f, $F_{\rm Ecl.}(f)$, i.e. the light removed from the composite spectrum due to the total eclipse, can be expressed as

$$F_{\rm Ecl.}(f) = F(f) - F_{\rm T}(f), \tag{2}$$

where $F(f)$ is the flux observed just prior to, or after the eclipse, and $F_{\rm T}(f)$ represents the flux measured during the totality. Having determined these fluxes from the corresponding magnitudes of the true continuum, we can write its colour indices in the form

$$U-B = -2.5\log\left(\frac{F_{\rm Ecl.}(U)}{F_{\rm Ecl.}(B)}\right) - (q_{\rm U}-q_{\rm B}) \tag{3}$$

and

$$B-V = -2.5\log\left(\frac{F_{\rm Ecl.}(B)}{F_{\rm Ecl.}(V)}\right) - (q_{\rm B}-q_{\rm V}), \tag{4}$$

where the constants $q_{\rm U}=38.40$, $q_{\rm B}=37.86$ and $q_{\rm V}=38.52$ define the magnitude zero for the standard Johnson *UBV* photometric system and fluxes in units of $\mathrm{J\,s^{-1}\,cm^{-2}\,\AA^{-1}}$ (Henden & Kaitchuck 1982). Because of brighter/fainter magnitudes are observed just prior/after the 2009 and 2007 eclipses, we considered both cases. In the $(U-B,\ B-V)$-diagram, the arrows start from the colour indices of the light produced by the eclipsed region at the beginning of the totality and point the position given by the eclipsed light at the end of the totality (left panel of Fig. 3). The observed U, B and V magnitudes during the 2009 total eclipse were 12.93, 13.02 and 11.59 (Fig. 2), their dereddened and emission line corrected values are 11.82, 12.20 and 10.81, which correspond to the continuum fluxes $F_{\rm T}(U)=8.2\times10^{-14}$, $F_{\rm T}(B)=9.5\times10^{-14}$ and $F_{\rm T}(V)=1.85\times10^{-13}\,\mathrm{erg\,cm^{-2}\,s^{-1}\,\AA^{-1}}$. Similarly we determined $F(U,B,V)$ fluxes from magnitudes prior to and after eclipses, and thus, according to Eq. (2), the $F_{\rm Ecl.}(U,B,V)$ fluxes. Using Eqs. (3) and (4) we inferred colour indices of the eclipsed light as $(U-B)_{2009}=-0.89$, $(B-V)_{2009}=0.56$ and $(U-B)_{2009}=-0.57$, $(B-V)_{2009}=0.31$ at the beginning and the end of the 2009 total eclipse, respectively. Similarly, for the 2007 eclipse, we obtained $(U-B)_{2007}=-1.44$, $(B-V)_{2007}=0.59$ and $(U-B)_{2007}=-1.32$, $(B-V)_{2007}=0.46$, respectively.

Table 3. Effect of emission lines on the $UBVR_C$ magnitudes

Date	ΔU_l	ΔB_l	ΔV_l	$\Delta R_{C,l}$
2007/11/20	–	-0.26	-0.07	-0.20
2007/12/03	-0.14	-0.24	-0.05	-0.15
2008/07/07	-0.10	-0.30	-0.06	-0.20
2008/08/10	-0.11	-0.33	-0.07	-0.22
2008/09/24	-0.12	-0.34	-0.07	-0.24
2008/10/23	-0.20	-0.35	-0.08	-0.25
2008/11/08	–	-0.34	-0.07	-0.24
2008/12/08	-0.18	-0.32	-0.06	-0.21
2009/03/24	–	-0.19	-0.05	-0.13
2009/04/01	–	-0.15	-0.06	-0.12
2009/04/07	–	-0.17	-0.05	-0.12
2009/04/08	–	-0.20	-0.05	-0.12
2009/04/09	–	-0.21	-0.06	-0.14
2009/04/14	–	-0.19	-0.06	-0.12
2009/05/05	–	-0.14	-0.04	-0.10
2009/08/05	-0.15	-0.23	-0.06	-0.10
2010/08/07	–	-0.30	-0.07	-0.22
2009/08/26	-0.10	-0.21	-0.07	-0.13
2009/09/24	–	-0.15	-0.06	-0.13
2010/08/16	-0.18	-0.36	-0.08	-0.27
2010/09/14	-0.22	-0.39	-0.10	-0.31

(iii) To diagnose the puzzling wave in the LC, we assumed that the observed continuum was composed of a variable and constant part of the light. Then the variable fraction, $F_{\rm var}(f)$, of the total continuum, $F_{\rm total}(f)$ can be written as

$$F_{\rm var}(f) = F_{\rm total}(f) - F_{\rm g}(f), \quad (5)$$

where the $F_{\rm g}(f)$ flux represents the (presumably) constant light of the giant measured throughout the filter f. First, to get magnitudes of the line-removed spectrum, we used average corrections from Table 3 as $\Delta U_{\rm l} = -0.11$, $\Delta B_{\rm l} = -0.20$, $\Delta V_{\rm l} = -0.05$, $\Delta R_{C,l} = -0.13$ and $\Delta I_{C,l} \equiv 0$. Second, we subtracted the light of the giant from the magnitudes of the true continuum. For the M4.5 III giant in AX Per (Mürset & Schmid 1999) we adopted colour indices as $U-B = 1.59$, $B-V = 1.57$ (Cox 2000) and $V-I_C = 2.76$, $R_C-I_C = 1.57$ (Bessell 1979) and its magnitude, $V_g \sim 11.13$, as results from our analysis of the UBV magnitudes presented in Sect. 3.1.4. The colour indices of the variable light then can be obtained from Eqs. (3) and (4) by substituting the $F_{\rm Ecl.}(f)$ flux by the $F_{\rm var}(f)$ one. The result is shown in the right panel of Fig. 3. We analyzed 24 UBV magnitudes between 2007/07/15 and 2009/03/14. To visualize better the result, we divided the data into 2 parts, with magnitudes $U < 12$ (filled squares in the figure) and $U > 12$ (open squares). Corresponding positions in the diagram imply that the variable part of the light consists of a nebular and stellar component of radiation. During the minima, the stellar component was very faint, because indices are clustered more around the line of the net nebular radiation, while during the maximum of the light wave, the stellar contribution became stronger. Analyzes of the UBV magnitudes (Sect. 3.1.4.) and modeling the SED (Sect. 3.2.3) support the result of the colour-diagram diagnostic.

3.2. Spectroscopic evolution

3.2.1. The line spectrum

During the investigated period of the 2007-10 activity, the optical spectrum of AX Per was dominated by H I, He I and He II emission lines, although some faint emissions, produced by permitted transitions in ionized metals, as e.g. N III 4641 and C III 4647 Å, were also present. Spectrum of forbidden lines was characterized mainly by nebular lines of [O III], [Ne III] and two [Fe VII] lines at 5721 and 6087 Å. The Raman-scattered O VI 1032 line was not present at all. Figure 4 shows evolution in the line profiles of He II 4686 Å, Hβ, Hα, [O III] 5007 Å and [Fe VII] 6087 Å, as observed on our high-resolution spectra. Figure 5 demonstrates variations in the line fluxes along the active period, as observed in all our spectra. Their quantities are introduced in Table 4 (available online).

Hydrogen lines: Profiles of hydrogen Balmer lines were significantly affected by a blue shifted absorption component. Its presence can be recognized around the whole orbital cycle. From the orbital phase $\varphi = 0.85$ to $\varphi = 1.19$, it created a double-peaked profile (Fig 4). In contrast, during the previous quiescent phase, the Hα line observed at similar orbital phases ($\varphi = 0.81$ and $\varphi = 0.16$, as on 1998 Jan. 9 and Sept. 5, respectively, see Fig. 5 in Skopal et al. 2001), did not display the double-peaked profile. In addition, both the total flux and the extension of the broad wings of, mainly, the Hα profile, were significantly larger than those measured during quiescent phase (Fig. 6 and Sect. 3.2.2 below). It is important to note that during the major 1988-91 outburst of AX Per, a strong absorption cut the broad emission profile even at positions with the hot star in front (see Figs. 5 and 8 of Ivison et al. 1993). This indicates the presence of neutral material on the line of sight around the whole orbit, which attenuates line photons via the $b-b$ transitions. The absorbing matter has to be located mostly at/around the orbital plane, because of its high inclination with respect to the observer. The strong difference in the line profiles, as measured during active and quiescent phases, suggests that the density of the neutral scattering material enhances during active phases at the orbital plane. Further, radial velocities (RV) of the absorption cores were negative with respect to the systemic velocity, and decreased in absolute values to higher members of the Balmer series. For example, on 2009 April 14th, we measured RV(Hα) = -143 km s^{-1}, RV(Hβ) = -138 km s^{-1}and RV(Hγ) = -103 km s^{-1}. Similar RVs of the hydrogen absorption components were revealed also during the major 1988-91 outburst by Ivison et al. (1993), who interpreted this effect as a result of a slowly expanding envelope. Finally, during the eclipse, total fluxes of Hα and Hβ lines, as well as their wings, decreased by a factor of > 3 with respect to their maximum values (Fig. 5, Table 4). The same behaviour was observed during the 1994 eclipse (see Fig. 6 of Skopal et al. 2001). Thus, during the active phases, the ionized region around the hot star, within the radius of the giant stellar disk, contributes significantly to the emission in hydrogen lines.

He II 4686 Å line: The He II 4686 Å emission line nearly disappeared during the eclipse. This allocates the region of its origin to the hot star vicinity, and constrains its maximum linear size to the diameter of the eclipsing giant. The measured flux in the He II 4686 line, F_{4686}, allow us to estimate the mean electron concentration in the He^{++} zone. Its luminosity in the He II 4686 line can be expressed as

$$4\pi d^2 F_{4686} = \alpha_{4686}(T_{\rm e}) n_{\rm e} n({\rm He}^{++}) h\nu_{4686} V_{4686}, \quad (6)$$

where $\alpha_{4686}(T_{\rm e})$ is the effective recombination coefficient for the given transition, $n_{\rm e}$ and $n(He^{++})$ is the mean concentration of electrons and He^{++} ions, respectively, and V_{4686} is the volume of the He^{++} zone. We further assume that all He atoms are fully

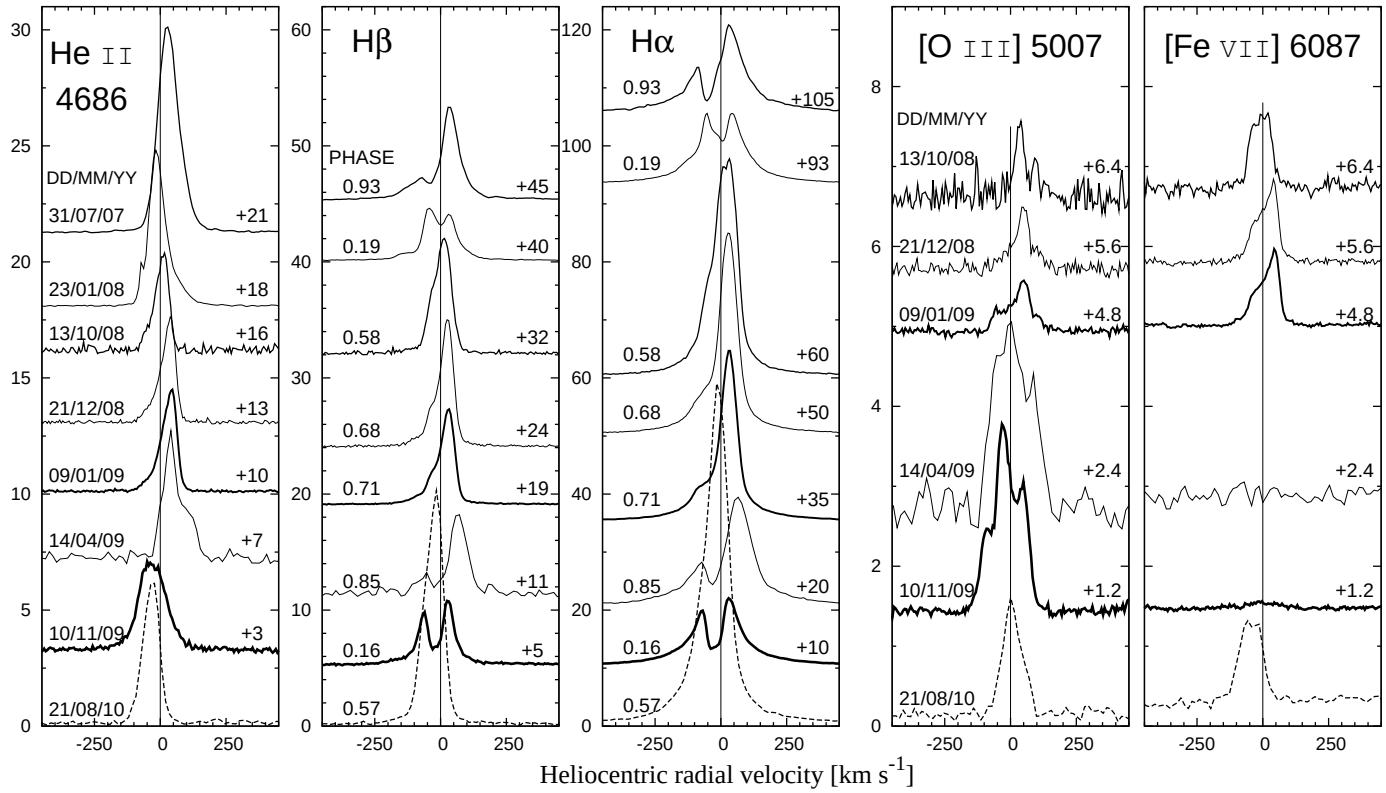

Fig. 4. Evolution in the selected line profiles along the 2007-10 active phase as observed on our high-resolution spectra. Fluxes are in units of 10^{-12} erg cm^{-2} s^{-1} Å^{-1}. Systemic velocity of –117.44 km s^{-1} was subtracted from radial velocities. Small numbers at the right side of panels represent a shift of profiles with respect to the level of the local continuum.

ionized within the zone, i.e. the abundance $A(\mathrm{He}^{++}) = A(\mathrm{He})$, and thus $n(\mathrm{He}^{++}) = A(\mathrm{He})n_\mathrm{p}$, because concentration of hydrogen atoms is equal to that of protons, n_p, in the ionized zone. Then the electron concentration

$$n_\mathrm{e} = (1 + 2A(\mathrm{He}^{++}))n_\mathrm{p}, \quad (7)$$

because each He atom produces 2 electrons within the He^{++} region. For $A(\mathrm{He}^{++}) = 0.1$ the ratio $n_\mathrm{p}/n_\mathrm{e} \sim 0.83$, and Eq. (6) can be expressed as

$$4\pi d^2 F_{4686} = \left(\frac{4}{3}\pi R_\mathrm{G}^3 \epsilon\right) \alpha_{4686}(T_\mathrm{e}) A(\mathrm{He}) n_\mathrm{e}^2 0.83 h\nu_{4686}, \quad (8)$$

where we approximated the V_{4686} volume by a sphere with the radius of the eclipsing giant, R_G, and ϵ is the filling factor. Our measured fluxes, $F_{4686} \sim 1.56 \times 10^{-11}$ and $\sim 7 \times 10^{-12}$ erg cm^{-2} s^{-1}, produced by the He^{++} zone prior to and after the eclipse, respectively (Fig. 5, Table 4), $\alpha_{4686}(30\,000\,\mathrm{K})h\nu_{4686} = 4.2 \times 10^{-25}$ erg cm^3 s^{-1} (Hummer & Storey 1987), $R_\mathrm{G} = 115\,R_\odot$ (Sect. 3.1.2.) and $\epsilon = 1$, yield a minimum $n_\mathrm{e} = 8.6 \times 10^9$ and 5.7×10^9 cm^{-3} during the 2009 brightening, prior to and after the eclipse, respectively. The size of the He^{++} zone can also be estimated from spectroscopic observations made close to the T_3 time (spectrum 26/08/2009) and just after the T_4 time (24/09/2009), when the He II 4686 line also aroused from the eclipse (Fig. 5). This time interval (~30 days) corresponds to $R_{4686} \sim 50\,R_\odot$, which yields $n_\mathrm{e} \sim 2.0 \times 10^{10}$ cm^{-3}.

Forbidden lines: In contrast to H and He lines, the nebular N_1 and N_2 ([O III] 5007 and 4959 Å) lines were not subject to the eclipse. Fluxes of the stronger 5007 Å line were as low as $\approx 1 \times 10^{-12}$ erg cm^{-2} s^{-1} prior to 2009 March, when increased to $\sim 4.5 \times 10^{-12}$ erg cm^{-2} s^{-1}, following the increase in the optical continuum. However, during the eclipse, the line flux persisted at the same level (Fig. 5). In 2010 it returned to the pre-brightening values. The ratio $R = F(N_1 + N_2)/F_{4363}$, which is a well known probe of n_e and T_e in planetary nebulae, was extremely low. The observed values, 0.5 – 2, imply a superdense [O III] nebula with n_e([O III]) $\sim 10^7 - 10^8$ cm^{-3} and T_e([O III]) < 20 000 K (e.g. Fig. 15.1 in Gurzadyan 1997). A detailed application of the method can be found in Skopal et al. (2001), who derived upper limit of n_e([O III]) as 7×10^7 cm^{-3} for $R = 1.7 - 4.3$. It is of interest to note that during the 1994 eclipse, fluxes in the N_1 and N_2 lines faded by a factor of ≤2 with respect to their out-of-eclipse values (see their Fig. 6 and Table 4), in contrast to the evolution during the 2009 eclipse. We discuss this interesting effect in Sect. 4.1.1.

The highly ionized [Fe VII] 6087 Å line was present in the spectrum only during a lower level of the activity. From the optical brightening in 2009 March to our last observation in 2009 November 10, when this line began to be detectable at $\approx 2 \times 10^{-15}$ erg cm^{-2} s^{-1} (Table 4), it disappeared from the spectrum entirely. Its profile was rather broad with $FWHM \sim 2.3$ Å and negative radial velocities of –18.1, –9.0, –7.3 and –53.9 km s^{-1} as on 2008/10/13, 2008/12/21, 2009/01/09 and 2010/08/21, respectively (systemic velocity of –117.44 km s^{-1} was subtracted). However, their peaks observed on 2008/12/21 and 2009/01/09 were placed at 24.8 and 25.8 km s^{-1} with a good agreement with those measured by Iijima (1988) (see his Fig. 4).

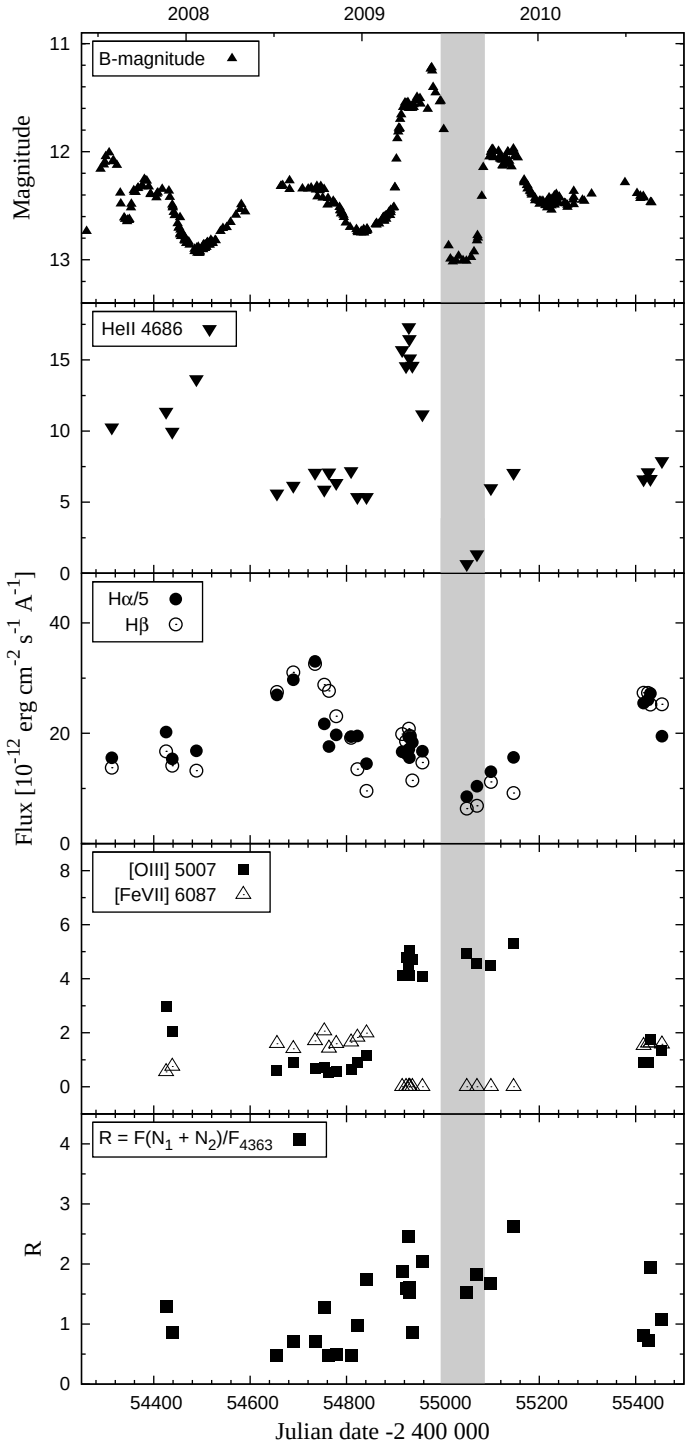

Fig. 5. Variation in the selected line fluxes during the 2007-10 active phase. Top panel shows the *B*-band LC to compare variation in the continuum and to visualize better the time-interval of the eclipse (the shadow band).

3.2.2. Mass loss through the hot star wind

During active phases the hot components in symbiotic binaries can lose their mass in the form of wind (e.g. Vogel 1993; Nussbaumer et al. 1995; Eriksson et al. 2004; Kenny & Taylor 2005; Skopal 2006). To estimate its rate we used the Hα method. Assuming that the broad Hα wings originate in the ionized wind from the hot star, we fitted their profile with a model of a bipolar stellar wind at the optically thin limit as proposed by Skopal (2006). The main aim of the modeling is to estimate the mass-loss rate via the hot star wind. Principle of the method is a comparison of the observed and synthetic profile of the broad wings.

The model assumes a spherically symmetric wind originating at the central star, covered by an optically thick disk in the direction of the observer. The disk is characterized with the radius $R_{\rm D}$ and height H, and it is seen edge-on in the model. Densities, and thus the emissivity of the wind at a given distance r from the hot star, is determined by the mass loss rate and the velocity of the wind. The velocity distribution is approximated with (Castor et al. 1975)

$$v(r) = v_\infty(1 - R_{\rm w}/r)^\beta, \qquad (9)$$

where the origin of the wind, $R_{\rm w}$, and β are model parameters, while the terminal velocity, v_∞, is given by the extension of the wings. During quiescent phase, parameters $R_{\rm D}$ and H can be estimated from the effective radius of the hot star, $R_{\rm h}^{\rm eff} \sim 0.1\,R_\odot$ (Table 3 of Skopal 2005). Assuming the ratio $H/R_{\rm D} = 0.1$ yields $R_{\rm D} = 0.32\,R_\odot$ and $H = 0.032\,R_\odot$. During the investigated active phase, we estimated the disk radius from the first two contact times of the 2009 eclipse (Sect. 3.1.2.) as $R_{\rm D} \sim 20\,R_\odot$. Assuming a flared disk with $H/R_{\rm D} = 0.3$, yields $H = 6\,R_\odot$. We remind here that the results do not depend critically on these parameters. The mass-loss rate is determined mainly by the luminosity of the broad wings and their terminal velocity (see Eq. (14) of Skopal 2006). Examples of comparison between the modeled and observed profiles are shown in Fig. 6. Synthetic profiles match well the observed wings for $|RV| \gtrsim 200 - 250\,{\rm km\,s^{-1}}$. There is a significant difference between the extension and luminosity of the Hα wings observed during quiescent and active phase (Table 5, Fig. 6). Broad wings from the 1998 quiescence corresponded to the mass-loss rates of $\lesssim 1\times10^{-7}\,M_\odot\,{\rm yr^{-1}}$, while during the activity, it increased to $\approx 2-3\times10^{-6}\,M_\odot\,{\rm yr^{-1}}$.

In our model, the mass loss rate determines particle density at a given distance r from the origin of the wind according to the continuity equation as

$$n_{\rm w}(r) = \dot{M}_{\rm w}/4\pi r^2 \mu m_{\rm H} v(r), \qquad (10)$$

where the wind velocity, $v(r)$, is given by Eq (9), μ is the mean molecular weight and $m_{\rm H}$ is the mass of the hydrogen atom. Within the He^{++} zone, i.e. from the hot star to $r_{\rm HeII} \approx 50\,R_\odot$ (Sect. 3.2.1), the particle densities $n_{\rm w}(r)$ are in excellent agreement with those derived independently from the measured F_{4686} fluxes. For example, $\dot{M}_{\rm w} = 3\times10^{-6}\,M_\odot\,{\rm yr^{-1}}$ and $v_\infty = 2000\,{\rm km\,s^{-1}}$, yield $n_{\rm w}(20\,R_\odot) \sim 2.8\times10^{10}$ (i.e. $n_{\rm e} = n_{\rm w}/0.83 = 3.3\times10^{10}\,{\rm cm^{-3}}$), and $n_{\rm w}(50\,R_\odot) \sim 3.2\times10^{9}\,{\rm cm^{-3}}$ ($n_{\rm e} = 3.9\times10^{9}\,{\rm cm^{-3}}$). This implies that particles of the hot stellar wind give rise to the observed emission from the He^{++} zone.

3.2.3. Modeling the continuum spectrum

The observed continuum spectrum of symbiotic stars, $F(\lambda)$, can formally be expressed as a superposition of its three basic components (see Sect. 1), i.e.

$$F(\lambda) = F_{\rm G}(\lambda) + F_{\rm N}(\lambda) + F_{\rm H}(\lambda), \qquad (11)$$

where $F_{\rm G}(\lambda)$, $F_{\rm N}(\lambda)$ and $F_{\rm H}(\lambda)$ represent radiative contributions from the giant, nebula and a hot stellar source, respectively. Basic features of these components of radiation are well recognizable on our low-resolution spectra exposed from short wavelengths, $\lambda \gtrsim 3300$ Å. Most distinctive are molecular passbands

Table 5. Parameters of synthetic models of the broad Hα wings (R_w, β, v_∞), their luminosities observed for $|RV| \geq 200\,\mathrm{km\,s^{-1}}$, $L_\alpha(200)$, and corresponding mass-loss rates, $\dot{M}_w$.

Date dd/mm/yyyy	R_w [$R_\odot$]	β	v_∞ [km s^{-1}]	$L_\alpha(200)$ [$L_\odot$]	$\log(\dot{M}_w)$ [$M_\odot$ yr^{-1}]
Quiescent phase: $R_D = 0.32\,R_\odot$, $H_D = 0.032\,R_\odot$					
09/01/1998	0.027	1.75	1500	0.90	-7.04
05/09/1998	0.030	1.75	1600	0.88	-7.02
Active phase: $R_D = 20\,R_\odot$, $H_D = 6\,R_\odot$					
31/07/2007	5.20	1.75	2500	2.97	-5.52
23/01/2008	5.27	1.74	2500	2.13	-5.59
13/10/2008	5.40	1.75	1500	0.83†	-5.84
21/12/2008	5.45	1.72	2000	1.60	-5.70
09/01/2009	5.40	1.75	2000	1.40	-5.72
14/04/2009	5.25	1.73	2500	3.17	-5.49
10/11/2009	5.20	1.75	2100	1.42†	-5.67
21/08/2010	0.94‡	1.80	2000	2.25†	-5.96

† $|RV| = 250\,\mathrm{km\,s^{-1}}$, ‡ $R_D = 3.5\,R_\odot$, $H_D = 1.05\,R_\odot$

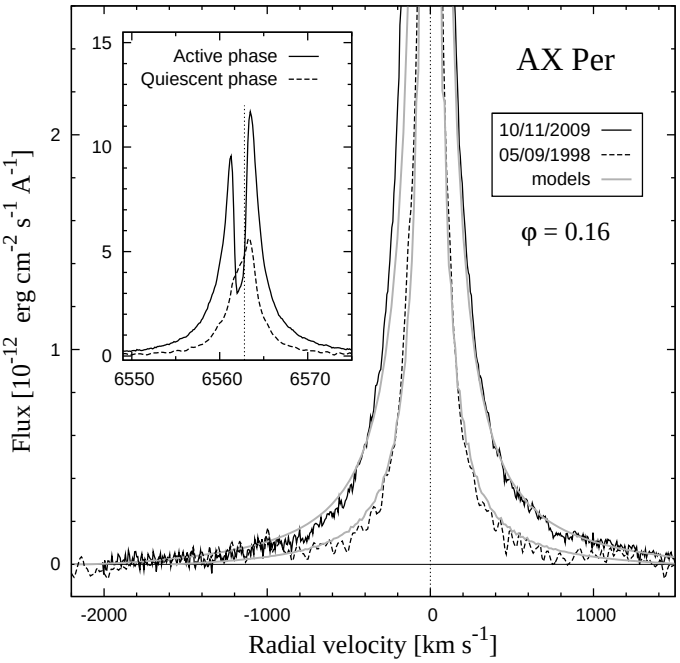

Fig. 6. Example of the broad Hα wings from the 2007-10 active phase (solid line), compared with that observed during quiescent phase (dashed line). Both spectra were taken at the same orbital phase, φ = 0.16. Local continua were subtracted from the spectra. The models (gray lines) indicate enhancement of the mass loss rate from $\sim 9\times10^{-8}$ to $\sim 3\times10^{-6}\,M_\odot\,\mathrm{yr^{-1}}$ from quiescence to activity (Table 5, Sect. 3.2.2).

arising in the red giant atmosphere, while a pronounced Balmer jump in emission indicates directly the presence of a strong nebular continuum. A hot stellar source of ionizing photons is indicated indirectly throughout the presence of strong recombination lines superposed to the continuum. Its direct indication is possible only within the super-soft X-ray and far-UV; in the optical its contribution is negligible (e.g. Fig. 2 of Skopal et al. 2009b). Another, significantly cooler stellar source of radiation develops during active phases. It is connected with the accretor, and its evidence is given directly by eclipses in the optical LCs (e.g. Belyakina 1979; Skopal 1991) and/or by model SED at any other orbital phase (Skopal 2005).

The aim of this section is to disentangle the composite spectrum, observed at different stages of AX Per activity, into its individual components of radiation, i.e to determine their physical parameters. For the $F_G(\lambda)$ component we used photospheric synthetic spectra of M-giant stars as published by Fluks et al. (1994). These models were calculated in the spectral range 350–900 nm for 11 spectral types (ST), from M0 to M10. In our modeling, we determine the ST and its subclass by a linear interpolation between the neighboring best fitting STs. As the radiation from the giant can vary, the scaling factor of the synthetic spectra represents another parameter in the model SED.

We approximated the spectrum produced by the nebula by

$$F_N(\lambda) = k_N \times \varepsilon_\lambda(T_e), \tag{12}$$

where k_N [cm^{-5}] is the scaling factor and $\varepsilon_\lambda(T_e)$ is the volume emission coefficient [erg cm^3 s^{-1} Å^{-1}], which depends on the electron temperature, T_e, and is a function of the wavelength (e.g. Brown & Mathews 1970). For the sake of simplicity, we calculated the $\varepsilon_\lambda(T_e)$ coefficient for the hydrogen plasma only, including contributions from recombinations and thermal bremsstrahlung. Some more arguments for such approximation are given in Skopal et al. (2009b). In addition, we assumed that T_e and thus $\varepsilon_\lambda(T_e)$ are constant throughout the nebula. Total emission produced by the optically thin nebula = $4\pi d^2 F_N(\lambda) = \varepsilon_\lambda \int_V n_e n_+ \mathrm{d}V = \varepsilon_\lambda EM$, where $EM = 4\pi d^2 k_N$ cm^{-3} is the emission measure of the nebula (see also Skopal 2005).

We compared the continuum of the hot stellar source to synthetic spectra based on Kurucz's codes as published by Munari et al. (2005). So, the third term of Eq. (11) can be written as

$$F_H(\lambda) = \theta_h^2 \mathcal{F}_\lambda(T_{\rm eff}), \tag{13}$$

where $\mathcal{F}_\lambda(T_{\rm eff})$ is the flux emitted by the stellar source. Its effective temperature, $T_{\rm eff}$, and scaling factor, $\theta_h = R_h^{\rm eff}/d$, represent free parameters in our modeling. Other atmospheric parameters of synthetic spectra were fixed ($\log(g) = 2.5, [M/H] = 0, [\alpha/\mathrm{Fe}] = 0, v_{\rm rot} = 20$ km s^{-1}), and their resolution was accommodated to that of our low-resolution spectra.

Having defined individual components of radiation in Eq. (11), we prepared a grid of models for reasonable ranges of the fitting parameters (ST, its subclass and scaling for the giant; T_e and k_N for the nebular continuum; $T_{\rm eff}$ and θ_h for the hot

stellar source), and selected that corresponding to a minimum of the function

$$\chi^2 = \sum_{\rm i=1}^{\rm N} \left[\frac{(F^{\rm obs}(\lambda_{\rm i}) - F(\lambda_{\rm i})}{\Delta F^{\rm obs}(\lambda_{\rm i})} \right]^2 , \quad (14)$$

where $F^{\rm obs}(\lambda_{\rm i})$ are fluxes of the observed continuum, N is their number (1500 – 1800), $\Delta F^{\rm obs}(\lambda_{\rm i})$ are their errors, and $F(\lambda_{\rm i})$ are theoretical fluxes given by Eq. (11). Input flux-points were selected from the observed spectra by omitting emission lines and a spectral region from 3645 to ∼3740 Å, where hydrogen lines of the high members of Balmer series were blended, which did not allow us to identify the true continuum. For the flux uncertainties we adopted typical values of 10%.

Our resulting models of the AX Per composite continuum along its active, 2007-10, phase are shown in Fig. 7 and the corresponding parameters are given in Table 6. The presence of rather cool stellar source in the 3200–7500 Å spectrum is constrained by a low Balmer jump and high values of the observed fluxes in the blue part of the spectrum. To fit the small Balmer discontinuity and to fill in the large difference between the contribution from the giant and the observed spectrum for $\lambda \lesssim 5000$ Å, the third radiative component with a rather flat energy distribution throughout the optical was required. This component satisfies well the radiation from a stellar source with temperature of 5000-7000 K. The strongest stellar source developed during the 2009 brightening (top right panel of Fig. 7). The following eclipse interrupted the brightening by removing entirely the stellar component and a part of the nebular one from the spectrum (emission measure decreased by a factor of ≳3). Immediately after the eclipse, the stellar source aroused again in the spectrum together with a stronger nebular emission (see Fig. 7 and Table 6). Our last spectra from 2010 August and September were possible to fit without the warm stellar component, which signalized return of AX Per to quiescent phase. For a comparison, we implanted the last spectrum into the UV-IR SED from quiescence (adapted according to Fig. 21 of Skopal 2005) to demonstrate the negligible contribution of the hot ionizing star in the optical (bottom panel of Fig. 7). Finally, it is of interest to note that the spectrum from 2008/12/08, taken during the minimum preceding the brightening phase, was possible to fit successfully (i.e. with $\chi^2_{\rm red} < 1$) with contributions from the giant and nebula only. The stellar component was negligible in spite of a higher level of activity. Such the model SED is consistent with the suggestion of our colour-diagram diagnostic (Sect. 3.1.3, Fig. 3 right), that during minima of the puzzling wave in the LC, the variable part of the light (see Eq. (5)) is of the nebular nature.

4. Discussion

From 2007, AX Per entered a new active phase, in spite that no typical 2-3 mag brightening in the optical was observed (see Sect. 3.1.1). This event was connected with a significant change in the ionization structure in the binary during the transition from the preceding quiescent phase.

In the continuum, this was indicated by a distinctive change in the minimum profile observed at/around the inferior conjunction of the giant. During quiescence, the broad minima in the LC (e.g. E = 4 to 9 in Fig. 1) are caused by the orbital motion of extended ionized wind from the giant, which is partially optically thick (Skopal 2001). During active phase, the broad minima were replaced by narrow ones (eclipses), which suggests that a large fraction of the light produced by the nebula and the hot star was concentrated at/around the accretor.

In the line spectrum, we indicated a significant increase in the mass-loss rate via the hot star wind with respect to the quiescent phase (Sect. 3.2.2, Fig. 6, Table 5). For example, during the 2009 brightening, we measured the highest luminosity and extension of the Hα wings, which corresponded to the mass loss rate of $\sim 3 \times 10^{-6}\ M_\odot\ {\rm yr}^{-1}$.

4.1. Evolution of the ionized zone

Throughout the whole 2007-10 period we observed a strong nebular component of radiation in the spectrum (Sect. 3.2.3, Fig. 7, Table 6). A geometrical change of the main source of the nebular radiation was indicated by the change in the position and profile of eclipses, during the 2007 and 2009 inferior conjunction of the giant. The 2007 eclipse was shifted from the giant conjunction by $\sim -0.025 P_{\rm orb}$. This implies that a strongly emitting region had to be located in front of the hot star, preceding its orbital motion. According to a gas-dynamical modeling of the mass-flow structures within the framework of the colliding winds model, a higher density region can develop about of 100-150 days after an increase of the hot star wind (see Figs. 4 and 5 of Bisikalo et al. 2006). Such the region will be ionized by the neighbouring hot star, and thus produce nebular emission. The nebular nature of the eclipsed light during the 2007.7 event (see left panel of Fig. 3, open pentagons marked with 2007) supports strongly this scenario. During the following conjunction in 2009.6, the eclipsed light resulted from a combination of both, the stellar and nebular component (Fig. 3 left, 2009 pentagons; Fig. 7 right: 2009/04/14 and 2009/09/24 SED), and the minimum was located exactly at the giant inferior conjunction (Fig. 2). As the nebular continuum was very strong during that time (Table 6), its dominant source also had to be located symmetrically around the hot star, and thus can be identified with its enhanced stellar wind. We remind here that our modeling of the broad Hα wings, whose profiles satisfy kinematics of the ionized stellar wind (Sect. 3.2.2), also supports location of the main source of the nebular emission around the hot star in a form of the wind.

4.1.1. Nebular lines

Spectroscopic observations made after the major 1989-91 active phase, at/around the 1994 eclipse, showed that the nebular [O III] lines were subject to eclipse. Their fluxes faded by a factor of ∼2 with respect to values, measured prior to and after the eclipse (see Table 4 of Skopal et al. 2001). In contrast, from 2009 March, nebular [O III] line fluxes increased by a factor of ∼4.5 and kept their values at a constant level to our last 2009 observation (2009/11/10), i.e. also throughout the eclipse (Fig. 5). This behaviour implies that the hot star wind gives rise to a significant fraction of the [O III] region. Its location is thus a function of the mass-loss rate, which determines particle densities at a given distance from the wind source. Higher $\dot{M}_{\rm w}$ places the [O III] zone to larger distances from the hot star and vice versa. During active phase, $\dot{M}_{\rm w} \sim 2 \times 10^{-6}\ M_\odot\ {\rm yr}^{-1}$, $v_\infty = 2000\ {\rm km\,s}^{-1}$ and critical densities for creation of nebular lines, $n_{\rm e} \gtrsim 10^7\ {\rm cm}^{-3}$, place the [O III] zone to distances $r > 210\ R_\odot$ from the accretor, i.e. far beyond the eclipsed region. However, durig quiescence, $\dot{M}_{\rm w} \sim 1 \times 10^{-7}\ M_\odot\ {\rm yr}^{-1}$ and $v_\infty = 1600\ {\rm km\,s}^{-1}$ (Table 5), shrink the critical radius to ∼50 $R_\odot$, which thus can be partially eclipsed by the giant with $R_{\rm G} \sim 115\ R_\odot$. Finally, the [O III] line

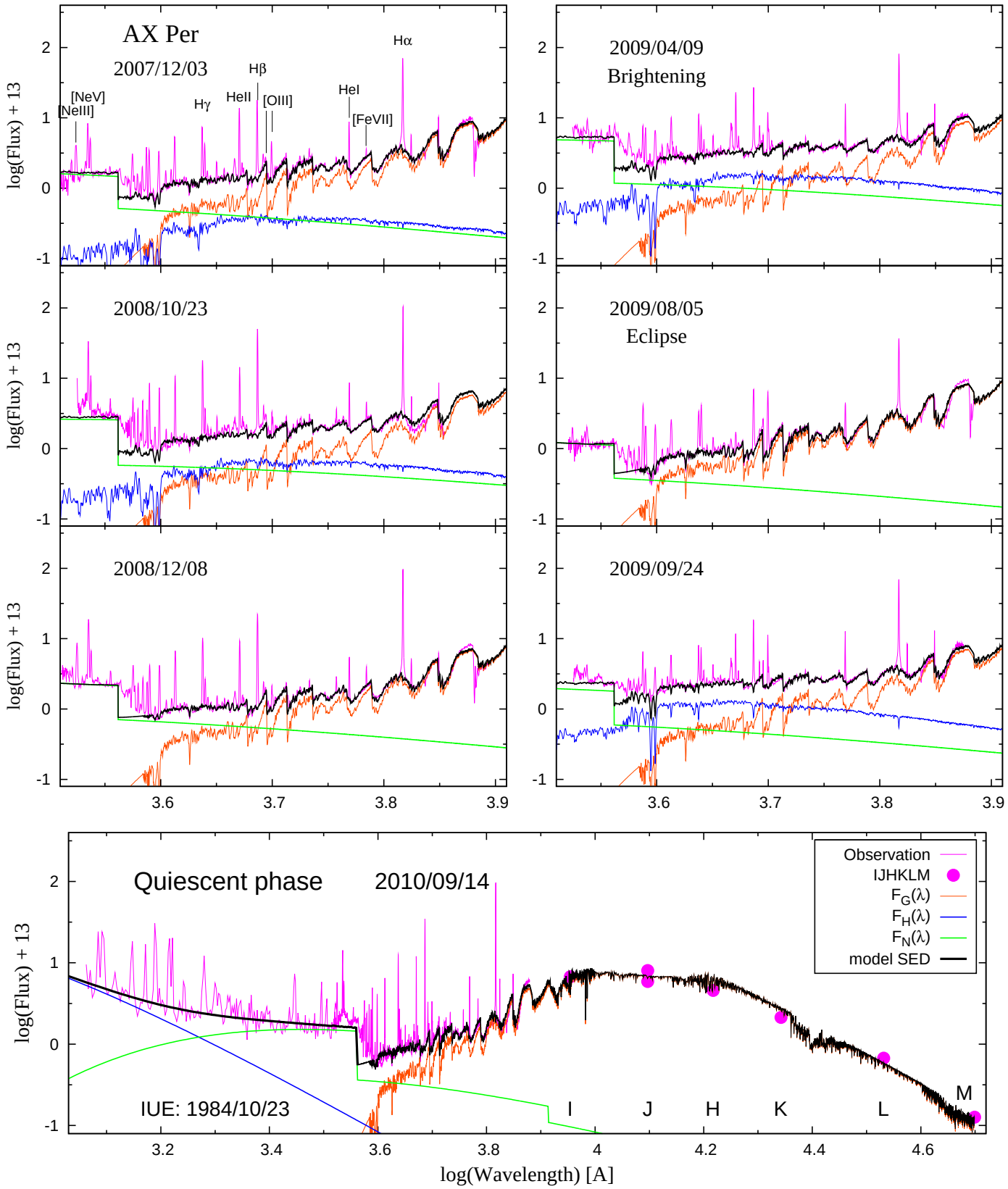

Fig. 7. Our low-resolution spectra (violet lines) and their models (black lines) at selected dates during the 2007-10 active phase of AX Per. The model SEDs and their components of radiation here represent a graphic form of Eq. (11) with the same denotation in keys. Fluxes are in units erg cm^{-2} s^{-1} Å^{-1}. Corresponding parameters are collected in Table 6. Modeling is described in Sect. 3.2.3.

Table 6. Parameters of the SED-fitting analysis (see Sect. 3.2.3, Fig. 7).

Date	Stage/B-mag	Giant		Hot object			Nebula		$\chi^2_{\rm red}$
dd/mm/yyyy		Sp. type	$T_{\rm eff}$/K†	$T_{\rm h}$/K	$R_{\rm h}^{\rm eff}/R_\odot$	$L_{\rm h}/L_\odot$	$T_{\rm e}$/K	$EM/10^{59}$ cm^{-3}	
03/12/2007	A / 12.5	5.8	3316	5250	6.2	26	34 000	3.5	0.75
23/10/2008	A / 12.4	5.8	3316	5250	8.2	45	23 000	3.8	1.17
08/12/2008	A / 12.7	5.8	3316	–	–	–	32 000	4.8	0.87
09/04/2009	A / 11.6	5.7	3326	5500	11	98	25 000	8.2	0.80
05/08/2009	A / 13.0‡	5.8	3316	–	–	–	33 000	2.6	0.78
26/08/2009	A / 12.8‡	5.6	3336	–	–	–	28 000	1.7	1.06
24/09/2009	A / 12.0	5.6	3336	6250	7.0	68	32 000	4.0	0.55
16/08/2010	Q / 12.4	5.3	3366	–	–	–	27 000	4.0	1.30
14/09/2010	Q / 12.5	5.3	3366	–	–	–	27 000	3.5	1.67

† according to the Fluks et al. (1994) calibration, ‡ eclipse

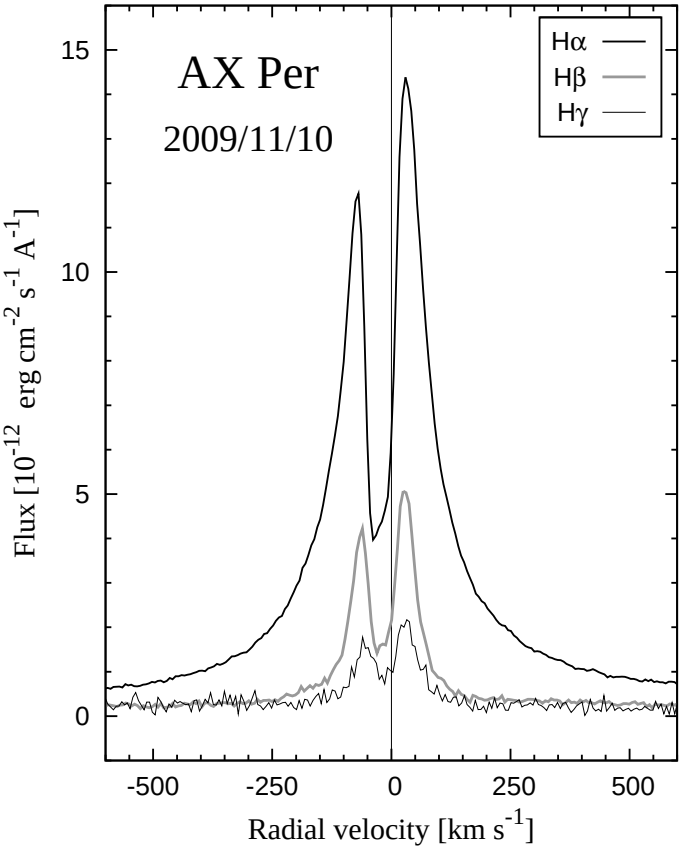

Fig. 8. Example of hydrogen line profiles of Balmer series. Systemic velocity of -117.44 km s^{-1} was subtracted. Blue-shifted absorption cores suggest a slow expansion of the neutral zone (see Sects. 3.2.1 and 4.2).

profiles consist of more components (Fig. 4), which suggests that the hot star wind, at further distances from its origin, was structured and not simply uniform in directions and densities.

4.2. Evolution of the neutral zone

We indicated the presence of a warm stellar component in the composite spectrum photometrically, by our colour-diagram diagnostic (Fig. 3) and by the 2009-eclipse profile, and spectroscopically, by disentangling the observed spectrum into its individual components (Fig. 7). Both analyzes are consistent. For example, just after the 2009.6 eclipse, the model SED (24/09/2009) suggested a dominant contribution from the warm stellar source (see Fig. 7), and the same was figured by our colour-diagram analysis at that time (Sect. 3.1.3, point (ii); Fig. 3 left, the corresponding 2009 pentagon lies close to the blackbody colour line).

Effective temperatures, ~5500 – 6500 K, radii of ~6 – 11 $R_\odot$ and luminosities between ~30 and 100 $L_\odot$ (Table 6) of the cool stellar source imply its non-spherical shape. (i) If this were a sphere, its radiation would not be capable of giving rise the observed nebular emission. On the other hand, the presence of the strong nebular componet in the spectrum constrains the presence of a hot ionizing source in the system, which is not seen directly in the optical. (ii) If the radius of the eclipsed object, $R_{\rm e} = 27\ R_\odot$ (Sect. 3.1.2), were that of a sphere, its luminosity would be a factor of ~15 larger than that we observed at the 2009 bright stage. These arguments suggest a disk-like structure of the hot active object with $R_{\rm D} = R_{\rm e}$. Assuming that its outer rim represents the cool pseudophotosphere (Sect. 5.3.5. of Skopal 2005), then its luminosity

$$2\pi R_{\rm D} 2H\sigma T_{\rm eff}^4 = 4\pi R_{\rm h}^2 \sigma T_{\rm eff}^4. \qquad (15)$$

For $H/R_{\rm D} \equiv 0.3$ (Sect. 3.2.2) and $R_{\rm h} = 11\,R_\odot$ (Table 6) we get $R_{\rm D} = 20\ R_\odot$, which is in good agreement with $R_{\rm e} = 22.3 \pm 2\ R_\odot$, obtained from the first two contact times of the 2009 eclipse. Thus, we conclude that the hot stellar object that developed during active phase has a form of a flared disk, which outer rim simulates the warm photosphere.

A comparison between the Hα profiles measured at the same orbital phase, but during quiescence and activity, reflects an increase of the density of neutral atoms of hydrogen on the line of sight during the active phase, i.e. at/around the orbital plane, because the binary is eclipsing and thus we see its orbit edge-on (Sect. 3.2.1, Fig. 6). Formation of the enhanced neutral scattering material at/around the accretor's equator is probably connected with the enhanced wind from the hot star during active phases. Observations constrain an optically thick wind in the hydrogen lines from the star's equator to a certain latitude, given by $R_{\rm D}$ and H parameters of the disk, where it becomes optically thin further to the star's pole (see the bipolar wind model of Skopal 2006). This suggestion is based on the SED analysis of active eclipsing symbiotics (Fig. 27 of Skopal 2005). The corresponding ionization structure then allows us to explain (at least qualitatively) the basic profile of hydrogen lines during activity, which consists of a central absorption core and extended emission wings. Radial velocities of central cores in Balmer lines reflect a slow expansion of the neutral zone (Sect. 3.2.1). The expansion accelerates from inner layers to outer ones, because the RVs of higher members of the Balmer series, which are created closer to the accretor, have a smaller negative velocity than the

lower members (Sect. 3.2.1, Fig. 8). Also, absorption cores are narrow even for higher members, which contradicts a fast, nearly Keplerian, rotation for the case of a standard accretion disk (e.g. Pringle 1981). This suggests that the neutral zone in the form of a disk, creating during active phase, has a different origin than a standard accretion disk in CVs. However, it is important to note that the absorption component from the neutral wind of the giant can also affect the central absorption core, mainly around the inferior conjunction of the giant. To recognize the origin of the central absorption in the Hα profile unambiguously, more observations along the orbit are needed to reconstruct the radial velocity curve (see e.g. Fig. 19 of Skopal et al. 1989).

4.2.1. Shaping of the neutral zone

From the beginning of the 2007-10 active phase, the LC was modified by a puzzling wave with a period of $\sim 0.5\,P_{\rm orb}$, broad minima located around orbital phases 0.2 and 0.7 and amplitude of $\sim 0.6 - 0.8$ mag (Fig. 2, Sect. 3.1.1). These properties suggest the presence of a strong, optically thick formation in the binary, which is located at the orbital plane and is prolonged from the orbital phase 0.2 to 0.7. Then its different projection into the line of sight at different binary positions could cause the observed wave-like variation.

We ascribe this formation to the neutral disk zone around the white dwarf (Sect. 4.2), which thus has to have an ellipsoidal shape with the major axis laying in the direction of the orbital phases 0.2 and 0.7. The neutral disk zone produces the warm stellar component of radiation. Its contribution to the composite spectrum is small during the optical minima in the LC (Sect. 3.1.3, point (iii); Figs. 3 and 7), which thus supports this interpretation.

5. Conclusions

In this paper we have investigated a new active phase of the eclipsing symbiotic binary AX Per, which began during 2007. Based on the results of our analyzes we formulate the following conclusions.

(i) AX Per entered a new active phase from ~2007.5 (Sect. 3.1.1). Our optical spectra and multicolour photometry revealed a significant change of the ionization structure in the binary with respect to the preceding quiescent phase (Sect. 4). For example, after 10 orbital cycles (~ 18.6 years) we measured again a deep narrow minimum in the LC, which was caused by the eclipse of the active star by its giant companion. We improved the ephemeris of eclipses (Eq. (1)), and found that their timing is identical (within uncertainties) with that of the inferior conjunction of the giant. We determined the radius of the giant as $R_{\rm g} = 115 \pm 2\,R_\odot$ and that of the eclipsed object, $R_{\rm e} = 27 \pm 2\,R_\odot$ (Sect. 3.1.2).

(ii) New active phase was connected with a significant enhancemet of the hot star wind. From quiescence to activity, the mass loss rate increased from $\sim 9\times10^{-8}$ to $\sim 2\times10^{-6}\,M_\odot\,{\rm yr}^{-1}$, respectively (Sect. 3.2.2, Table 5, Fig. 6). The mean electron concentration within the eclipsed He^{++} zone ($R_{\rm HeII} \sim 50\,R_\odot$ above the hot star), $\sim 10^{10}\,{\rm cm}^{-3}$, is in good agreement with that given independently by the mass loss rate (Sects. 3.2.1 and 3.2.2). The hot star wind gives rise also to a significant fraction of the [O III] zone. Depending on the mass-loss rate, the nebular lines can be subject to partial eclipse (1994 eclipse) or not (2009 eclipse; Sects. 4.1.1).

(iii) Based on model SEDs (Sect. 3.2.3, Fig. 7), colour-diagram diagnostic (Fig. 3) and the eclipse profile, we identified a warm stellar source located at the hot star's equator, which developed during the 2007-10 active phase. The source had a form of a flared disk, which outer rim simulated the warm photosphere. Its formation was connected with the enhanced wind from the hot star (Sect. 4.2). Probably, this connection represents a common origin of cool pseudophotospheres indicated during active phases of symbiotic stars.

Acknowledgements. The authors would like to thank Theodor Pribulla for acquisition of spectra at the David Dunlap Observatory. We also would like to thank S. Bacci, M. Marinelli, L. Ghirotto, A. Milani for assistance with some of the photometric and spectroscopic observations. We acknowledge with thanks the variable star observations from the AAVSO International Database contributed by observers worldwide and used in this research. This research was in part supported by a grant of the Slovak Academy of Sciences No. 2/0038/10.

References

Belyakina, T. S. 1979, Izv. Krym. Astrophys. Obs., 59, 133
Belyakina, T. S. 1991, Bull. CrAO, 83, 104
Bessell, M. S. 1979, PASP, 91, 543
Bisikalo, D. V., Boyarchuk, A. A., Kilpio, E. Yu., Tomov, N. A., & Tomova, M. T. 2006, Astron. Reports, 80, 722
Brown, R. L., & Mathews, W. G. 1970, ApJ, 160, 939
Castor, J. I., Abbott, D. C., & Klein R. I. 1975, ApJ, 195, 157
Cariková, Z. & Skopal, A. 2010, New A, 15, 637
Corradi, R. L. M., Mikolajewska, J., & Mahoney, T. J. 2003, Symbiotic Stars Probing Stellar Evolution, ASP Conf. Ser. 303 (San Francisco: ASP)
Cox, A. N. 2000, Allen's Astrophysical Quantities (New York: AIP Press)
Eriksson, M., Johansson, S., & Wahlgren, G. M. 2004, A&A, 422, 987
Fekel, F. C., Hinkle, K. H., Joyce, R. R., & Skrutskie, M. F. AJ, 120, 3255
Fluks, M. A., Plez, B., The, P. S., de Winter, D., Westerlund, B. E., & Steenman, H. C. 1994, A&AS, 105, 311
Fujimoto, M. Y. 1982, ApJ, 257, 767
Gurzadyan G. A., 1997, The Physics and Dynamics of Planetary Nebulae. Springer-Verlag, Berlin
Henden, A. A., & Kaitchuck, R. H. 1982, Astronomical Photometry, Van Nostrand Reinhold Company, New York
Henden, A. A., & Munari, U. 2006, A&A, 458, 339
Hummer, D. G. & Storey, P. J. 1987, MNRAS, 224, 801
Iijima, T. 1988, Ap&SS, 150, 235
Ivison, R. J., Bode, M. F., Evans, A., Skopal, A., & Meaburn, J. 1993, MNRAS, 264, 875
Kenny, H. T., & Taylor, A. R. 2005, ApJ, 619,527
Kenyon, S. J., & Webbink, R. F. 1984, ApJ, 279, 252
Mikolajewska, J. & Kenyon, S. J. 1992a, MNRAS, 256, 177
Mikolajewska, J. & Kenyon, S. J. 1992b, AJ, 103, 579
Munari, U., Buson, L. M. 1994, A&A, 287, 87
Munari, U., Sordo, R., Castelli, F., & Zwitter, T. 2005, A&A, 442, 1127
Munari, U., Siviero, A., Dallaporta, S., et al. 2009, CBET No. 1757
Munari, U., Siviero, A., Corradi, R. L. M., Valisa, P., Cherini, G., Castellani, F., & Dallaporta, S. 2010, CBET No. 2555
Mürset, U., & Schmid, H. M. 1999, A&AS, 137, 473
Nussbaumer, H., & Vogel, M. 1989, A&A, 213, 137
Nussbaumer, H., Schmutz, W., & Vogel, M. 1995, A&A, 293,13
Pereira, C. B., & Cunha, K. 2003, in ASP Conf. Ser. 303, Symbiotic Stars Probing Stellar Evolution, ed. R. L. M. Corradi, J. Mikolajewska, & T. J. Mahoney (San Francisco, CA: ASP), 359
Pacźynski, B., & Żytkow, A. N. 1978, ApJ, 222, 604
Paczyński, B., & Rudak, R. 1980, A&A, 82, 349
Pringle, J. E. 1981, ARA&A, 19, 137
Seaquist, E. R., Taylor, A. R., & Button, S. 1984, ApJ, 284, 202
Siviero, A., Munari, U., Dallaporta, S., et al. 2009, MNRAS, 399, 2139
Skopal, A. 1991, IBVS No. 3603
Skopal, A. 1994, A&A, 286, 453
Skopal, A. 2000, CoSka, 30, 21
Skopal, A. 2001, A&A, 366, 157
Skopal, A. 2003, Baltic Astronomy, 12, 604
Skopal, A. 2005, A&A, 440, 995
Skopal, A. 2006, A&A, 457, 1003
Skopal, A. 2007, New A, 12, 597
Skopal, A., Mikolajewski, M., & Biernikowicz, R. 1989, Bull. of Astron. Inst. Czechosl., 40, 333
Skopal, A., Teodorani, M., Errico, L., Vittone, A. A., Ikeda, Y., & Tamura, S. 2001, A&A, 367, 199

Skopal, A., Pribulla, T., Budaj, J., Vittone, A. A., Errico, L., Otsuka, M., Wolf, M., Chrastina, M., & Mikulášek, Z. 2009a, ApJ, 690, 1222
Skopal, A., Sekeráš, M., Gonzlez-Riestra, R., & Viotti, R. F. 2009b, A&A, 507, 1531
Skopal, A. et al. 2011, Astron. Nachr. (to be submitted)
Sokoloski, J. L. 2003, in ASP Conf. Ser. 303, Symbiotic Stars Probing Stellar Evolution, ed. R. L. M. Corradi, J. Mikolajewska, & T. J. Mahoney (San Francisco, CA: ASP), 202
Sokoloski, J. L., & Kenyon, S. J. 2003, ApJ, 584, 1021
Sokoloski, J. L., Kenyon, S. J., Espey, B. R., et al. 2006, ApJ, 636, 1002
Tutukov, A. V., & Yangelson, L. R. 1976, Astrofizika, 12, 521
Vogel, M. 1993, A&A, 274, L21
Zamanov, R. K., Bode, M. F., Melo, C. H. F., Porter, J., Gomboc, A., & Konstantinova-Antova, R. 2006, MNRAS, 365, 1215
Zamanov, R. K., Bode, M. F., Melo, C. H. F., Stateva, I. K., Bachev, R., Gomboc, A., Konstantinova-Antova, R., & Stoyanov, K. A. 2008, MNRAS, 390, 377

Appendix A: On-line material: Table 2

Appendix B: On-line material: Table 4

Table A.1. Table 2: Our B, V, R_C, I_C CCD photometric observations of AX Persei

Date yyyy/mm/dd	Julian date +2 450 000	B	V	B-V	V-R	V-I
2007/06/08	4260.547	12.736	11.503	1.170	1.278	3.089
2007/07/07	4289.514	12.161	11.063	1.009	1.076	2.717
2007/07/14	4296.448	12.121	10.988	0.961	0.980	2.734
2007/07/16	4298.448	12.097	10.998	0.971	1.026	2.785
2007/07/18	4300.466	12.044	10.947	0.945	1.036	2.619
2007/07/25	4307.415	12.010	10.987	0.943	0.961	2.695
2007/08/01	4314.473	12.092	10.999	0.963	1.127	2.723
.....	.....	.....	.....	.....	.....	.....
.....	.....	.....	.....	.....	.....	.....
.....	.....	.....	.....	.....	.....	.....
2010/08/01	5409.577	12.431	11.353	0.971	999	2.785
2010/08/07	5415.593	12.413	11.349	0.961	1.471	2.774
2010/08/08	5416.592	12.426	11.371	0.966	999	2.798
2010/08/22	5430.619	12.469	11.493	0.868	999	2.876
2010/08/24	5432.553	12.471	11.483	0.909	1.511	2.834

Table B.1. Table 4: Emission line fluxes in erg cm^{-2} s^{-1}

Date	Julian date +2 450 000	[OIII] 4363	HeII4686	Hβ	[OIII] 4950	[OIII] 5007	He I 5875	[FeVII] 6087	Hα	Res†
2007/07/31	4312.876	–	0.1027E-10	0.1375E-10	–	–	–	–	0.7778E-10	h
2007/11/20	4425.529	0.2692E-11	0.1138E-10	0.1673E-10	0.4850E-12	0.2981E-11	0.8335E-11	0.5535E-12	0.1011E-09	l
2007/12/03	4438.438	0.2405E-11	0.9972E-11	0.1412E-10	?	0.2067E-11	0.5967E-11	0.7494E-12	0.7677E-10	l
2008/01/23	4488.506	–	0.1367E-10	0.1322E-10	–	–	–	–	0.8410E-10	h
2008/07/07	4655.473	0.1323E-11	0.5628E-11	0.2748E-10	?	0.6226E-12	0.5542E-11	0.1594E-11	0.1348E-09	l
2008/08/10	4689.450	0.1283E-11	0.6174E-11	0.3104E-10	?	0.9025E-12	0.6602E-11	0.1406E-11	0.1485E-09	l
2008/09/24	4734.609	0.9510E-12	0.7088E-11	0.3256E-10	?	0.6724E-12	0.6455E-11	0.1697E-11	0.1652E-09	l
2008/10/13	4753.638	0.7731E-12	0.5899E-11	0.2880E-10	0.2676E-12	0.7186E-12	0.5223E-11	0.2060E-11	0.1085E-09	h
2008/10/23	4763.417	0.1115E-11	0.7103E-11	0.2769E-10	?	0.5218E-12	0.4928E-11	0.1421E-11	0.8801E-10	l
2008/11/08	4778.393	0.1109E-11	0.6367E-11	0.2310E-10	?	0.5525E-12	0.4105E-11	0.1593E-11	0.9858E-10	l
2008/12/08	4809.390	0.1309E-11	0.7203E-11	0.1918E-10	?	0.6316E-12	0.3453E-11	0.1648E-11	0.9701E-10	l
2008/12/21	4822.437	0.1268E-11	0.5378E-11	0.1349E-10	0.3315E-12	0.9129E-12	0.3583E-11	0.1825E-11	0.9757E-10	h
2009/01/09	4841.426	0.8753E-12	0.5379E-11	0.9558E-11	0.3465E-12	0.1178E-11	0.2453E-11	0.1987E-11	0.7248E-10	h
2009/03/24	4915.422	0.2726E-11	0.1571E-10	0.1985E-10	0.9929E-12	0.4114E-11	0.7603E-11	0	0.8329E-10	l
2009/04/01	4923.323	0.3561E-11	0.1458E-10	0.1855E-10	0.8831E-12	0.4800E-11	0.8640E-11	0	0.8165E-10	l
2009/04/07	4929.303	0.2187E-11	0.1732E-10	0.2083E-10	0.1019E-11	0.4365E-11	0.8459E-11	0	0.8557E-10	l
2009/04/08	4930.301	0.3125E-11	0.1648E-10	0.1939E-10	?	0.5029E-11	0.8348E-11	0	0.7790E-10	l
2009/04/09	4931.262	0.3532E-11	0.1513E-10	0.1952E-10	0.1285E-11	0.4112E-11	0.8451E-11	0	0.9625E-10	l
2009/04/14	4936.338	0.7458E-11	0.1461E-10	0.1145E-10	0.1656E-11	0.4710E-11	0.6371E-11	0	0.9172E-10	h
2009/05/05	4957.458	0.2389E-11	0.1120E-10	0.1471E-10	0.7640E-12	0.4100E-11	0.7413E-11	0	0.8370E-10	l
2009/08/05	5049.535	0.3234E-11	0.6719E-12	0.6353E-11	?	0.4926E-11	0.3008E-11	0	0.4250E-10	l
2009/08/26	5070.565	0.3085E-11	0.1359E-11	0.6866E-11	0.1055E-11	0.4582E-11	0.3347E-11	0	0.5199E-10	l
2009/09/24	5099.584	0.3314E-11	0.5999E-11	0.1118E-10	0.1105E-11	0.4474E-11	0.6023E-11	0	0.6519E-10	l
2009/11/10	5146.485	0.2615E-11	0.7074E-11	0.9168E-11	0.1538E-11	0.5314E-11	0.4716E-11	0.2061E-14	0.7812E-10	h
2010/08/07	5416.368	0.1096E-11	0.6622E-11	0.2735E-10	?	0.8840E-12	0.5056E-11	0.1521E-11	0.1274E-09	l
2010/08/16	5425.564	0.1244E-11	0.7124E-11	0.2732E-10	?	0.9043E-12	0.5392E-11	0.1611E-11	0.1303E-09	l
2010/08/21	5430.348	0.1490E-11	0.6655E-11	0.2520E-10	0.1160E-11	0.1743E-11	0.1356E-10	0.1612E-11	0.1361E-09	h
2010/09/14	5454.560	0.1545E-11	0.7908E-11	0.2525E-10	0.3326E-12	0.1332E-11	0.4801E-11	0.1574E-11	0.9732E-10	l

† h - high-resolution, l - low-resolution spectrum; ? - blended, not measurable line